Title:

Brain histone beta-hydroxy-butyrylation couples metabolism with gene expression

Sara Cornuti[1,6], Leonardo Lupori[1,6], Siwei Chen[2,6], Francesco Finamore[3], Muntaha Samad[2], Francesco Raimondi[1], Raffaele Mazziotti[4], Christophe Magnan[2], Silvia Rocchiccioli[3], Pierre Baldi[2], Tommaso Pizzorusso[1,4,†], Paola Tognini[1,5*,†]

1 BIO@SNS lab, Scuola Normale Superiore, Pisa, Italy.
2 Institute for Genomics and Bioinformatics, School of Information and Computer Sciences, University of California, Irvine, CA, USA.
3 Institute of Clinical Physiology, National Research Council, Pisa, Italy.
4 Department of Neuroscience, Psychology, Drug Research and Child Health NEUROFARBA University of Florence, Florence, Italy.
5 Department of Translational Research and New Technologies in Medicine and Surgery, University of Pisa, Pisa, Italy.
6 These authors contributed equally to this work

* Correspondence: paola.tognini@unipi.it
† Co-last authors

ABSTRACT

Metabolic status has a well-documented influence on peripheral organs' physiology and pathology, however mounting evidence suggests that it can also affect brain function. For example, brain resilience to aging is enhanced by caloric restriction, and ketogenic diets have been used to treat neurological diseases. Unfortunately, little is known about the impact of metabolic stimuli on brain tissue at a molecular level. Recent data obtained in liver tissue suggest that beta-hydroxybutyrate (BHB) can also be a key signaling molecule regulating gene transcription. Thus, we adopted a ketogenic metabolic challenge, based on 48 hrs of fasting, and then assessed lysine beta-hydroxybutyrylation (K-bhb) levels in proteins extracted from the cerebral cortex. We found that fasting enhanced K-bhb in a variety of proteins and on histone H3. ChIP-seq experiments showed that K9 beta-hydroxybutyrylation of H3 (H3K9-bhb) was significantly enriched by fasting on more than 8000 DNA loci. Transcriptomic analysis showed that H3K9-bhb on enhancers and promoters correlated with active gene expression. Since one of the most enriched functional annotations both at the epigenetic and transcriptional level was "circadian rhythms", we studied the expression of core-clock genes in the cortex during fasting.

We found that the diurnal oscillation of specific transcripts was modulated at distinct times of the day along the circadian cycle. Thus, our results suggest that fasting dramatically impinges on the cerebral cortex transcriptional and epigenetic landscape, and BHB acts as a powerful epigenetic molecule in the brain through direct and specific histone marks remodelling in neural tissue cells.

Keywords: fasting, cerebral cortex, beta-hydroxybutyrylation, transcriptome, epigenome

INTRODUCTION

Nutrition is emerging as a key regulator of whole-body physiology and health. Food impinges on tissue functions through modulation of metabolism, which results in adaptive changes in cellular biochemical/molecular processes, and ultimately tissue homeostasis. Notably, beside the well-documented influence on peripheral organs' physiology/pathology, mounting evidence shows that the metabolic status can also affect neuronal function and metabolism, and influence brain physiology and ultimately cognitive processes, emotions and behavior (1–3). Indeed, the high fat/high sugar western diet negatively affects brain health, leading to alterations in cognitive functions, anxiety, depression, and in general a higher incidence of emotional disorders (4, 5). On the other hand, caloric restriction has been shown to prevent age-related brain damage and to be neuroprotective by influencing free radical metabolism, and the cellular stress response system (6, 7). In 1920's very low carbohydrate/high fat ketogenic diets (KD) were introduced in the clinic to treat refractory epilepsy, mimicking the increase in the blood level of ketone bodies (i.e. beta-hydroxybutyrate (BHB)), which were thought to mediate the effect of fasting on seizure events (8). Notably, epilepsy has high comorbidity with neurodevelopmental disorders such as autism spectrum disorders (ASD), and KD is one of the therapeutic approaches proposed to treat ASD patients (9). KD seems also to be beneficial in the treatment of neurodegenerative and psychiatric diseases (10, 11). Finally, fasting and aerobic exercise may improve cognitive performance and protect against depression and anxiety-like behaviour through the enhancement of hippocampal neurogenesis (12, 13). Thus, in short, diet robustly influences neurological outcomes, yet the molecular and biochemical underpinnings of these effects are poorly understood.

KD, fasting or starvation, and prolonged aerobic exercise, all promote the depletion of liver glycogen stores, favouring the decrease of blood glucose concentration. Due to its scarcity, glucose cannot be used to respond to the energy request of organismal tissues. Thus, to maintain metabolic homeostasis, our body switches to an alternative fuel: ketone bodies, produced via the activation of the so-called ketogenic pathway. Mainly in the liver, the acetyl-CoA produced by fatty acid oxidation is converted into three ketone bodies: acetoacetate, acetone, and BHB. The latter is the most abundant circulating ketone body and, under ketogenic conditions, the major energy source for metabolic active tissues, such as the brain (14). Intriguingly, BHB is not just an energy carrier as it was believed in the past. Emerging evidence suggests that BHB is also a *signaling* molecule, capable of binding to the HCAR2 and FFAR3 receptors (15–17), and of acting as an endogenous epigenetic regulator. Indeed, BHB selectively acts as a class 1 Histone deacetylase inhibitor, increasing histone acetylation and

active gene expression (18). Finally, BHB is the chemical donor for a new epigenetic mark so far investigated in detail only in the liver: lysine beta-hydroxy-butyrylation (K-bhb). Liver K-bhb contributes to active gene expression and regulates genes involved in the hepatic metabolic response to starvation (19).

Despite the high ketone bodies demand of the brain, the impact of BHB on neural tissue epigenome and transcriptome has never been explored. To address this important issue, which could underline and shed light on the adaptation capability of neuronal circuits to nutritional changes, we analyzed *in vivo* neural tissue responses to a specific metabolic challenge consisting of 48-hours fasting. Specifically, we discovered that fasting enhanced K-bhb in a variety of proteins. Then, we explored the genome-wide distribution of K9-bhb on histone H3 (H3K9-bhb) through chromatin immunoprecipitation, followed by sequencing (ChIP-seq) in the occipital cortex (an area corresponding to the visual cortex) of fasted (F) mice, and parallel measurement of the transcriptional response through RNA-seq. Dataset crossing pointed toward H3K9-bhb being an epigenetic mark related to fasting-induced gene expression, therefore suggesting that fasting-driven increase in BHB could directly affect brain cells through remodeling of the chromatin landscape and transcriptional responses.

RESULTS

Fasting driven-increase in BHB causes a burst in protein Lysine beta-hydroxybutyrylation in the brain.

To assess the molecular response of brain tissue to fasting-induced ketosis, we adopted a protocol of prolonged fasting and we assessed the biochemical action of a major metabolite produced upon fasting: BHB (Fig. 1A)**.** Postnatal day (P) 33 mice were subjected to a fasting (F) condition, corresponding to a total absence of food for 48 hours (48h), but ad libitum (AL) access to water. Their body weight and glycemia were monitored before and after fasting. F mice displayed a significant decrease in their body weight and in blood glucose concentration after 48h, while AL control mice did not show any significant difference (Fig. 1 B-C). During the 48 h of food deprivation, F animals displayed a significant increase in spontaneous locomotor activity both during night and day time (Fig. 1D), showing that our protocol did not cause lethargy in the subjects and confirming behavioral changes reflecting the search for food (20).

Since BHB has been demonstrated to be the chemical moiety for a new post-translational modification (PTM) on K residues (19), we performed a western-blot analysis of protein extract

from the occipital cortex of F and AL mice using a pan-K-bhb antibody. Strikingly, K-bhb was significantly increased in the occipital cortex of F mice with respect to AL (Fig. 2A), suggesting that the increased cortical BHB after fasting could be exploited, not only to produce energy, but also as a chemical donor for PTM. As a control, we analysed the pan-K-bhb in the liver of the same mice, and confirmed a significant upregulation in F mice with respect to AL (Suppl. Fig. 1A).

HPLC-MS analysis of K-bhb residues in protein extract from the occipital cortex highlighted the presence of 234 beta-hydroxybutyrilated proteins. In total, 137 proteins were beta-hydroxybutyrilated exclusively in F mice, 77 proteins exclusively in AL mice, and 20 proteins were beta-hydroxybutyrilated in both groups (Fig. 2B). The 20 common beta-hydroxybutyrilated proteins were enriched in annotations such as “NADP metabolic processes” ans “positive regulation of fibroblast proliferation”'(Fig 2B and Dataset S1). On the other hand, the F proteins displaying K-bhb clustered in specific GO annotations mainly related to “regulation of transcription, regulation of transcription dependent on RNA pol II and morphogenesis” (Fig. 2B and Dataset S2). Also, the GO biological processes analysis of the proteins beta-hydroxybutyrilated in AL indicated an enrichment in “transcription, and chromatin modification” annotations (Fig. 2B, and Dataset S3). These findings suggest that BHB may have a more complex function related to transcriptional regulation, not just limited to HDAC inhibition or being a chemical moiety for histone PTMs, but also associated with the modulation of epigenetic (e.g. KDM1B, HDAC2), transcription factors (e.g.E2F4, HOXB3) or other chromatin-related proteins (e.g. SKOR1, CHD5) functions.

BHB has been demonstrated to modify K-bhb on histones with consequent alteration of the liver transcriptional program (19). Thus, we studied K9-bhb on histone H3 (H3K9-bhb) in the brain using a specific and commercially available antibody. H3K9-bhb was significantly more abundant in the cortex of F mice (Fig. 2C) with respect to the AL group. As expected, H3K9-bhb increased also in the liver of F mice (Suppl. Fig. 1B).

Overall, these data demonstrate that beta-hydroxybutyrylation is conspicuously enhanced by fasting in neural tissue.

BHB impacts the chromatin state of the cerebral cortex through a direct epigenetic action

To further explore the role of H3K9-bhb in the CNS, we performed a ChIP-seq experiment and studied the genome-wide distribution of H3K9-bhb in the visual cortex of mice subjected to 48h fasting or fed AL. The ChIP-seq analysis revealed a striking increase in H3K9-bhb enriched loci in F with respect to AL. Indeed, the differential analysis between the two experimental

conditions detected about 8400 enriched peaks ($p<0.05$) in F vs AL (Dataset S4) distributed in intergenic (42%), promoter (17%), and enhancer regions (18%, Fig. 3A).

To gain further insight into the specific epigenetic effects of BHB in neural tissue, we crossed our H3K9-bhb ChIP-seq data with the already published H3K9-bhb ChIP-seq data in the liver (19). The analysis of the data in Xie et al., with our pipeline (see materials and methods) revealed that the total number of H3K9-bhb peaks in the brain was lower than in the liver (8404 brain loci vs 15416 liver loci). Peak category distribution demonstrated that H3K9-bhb was principally present in promoter and enhancer regions in the mouse liver after 48h fasting (Suppl. Fig. 2), while enhancer, promoter, and especially intergenic regions were the most prominent category in the brain (Fig. 3A). In the cerebral cortex, the GO “biological processes” analysis of the genes in proximity of promoters and enhancer regions (Datasets S5 and S6) highlighted a specific signature related to circadian rhythms, and pathways involving histone PTM and chromatin remodelling (Fig. 3B-C). Also, synaptic transmission, dendrite morphogenesis, and synapse assembly came up as enriched GO terms associated with the enhancer regions. Brain neurogenesis, brain and dendrite morphogenesis, and axon guidance terms were dominant among the genes associated with the promoter regions (Dataset S5). The KEGG pathway analysis in the enhancers confirmed the “circadian rhythms” and “synaptic transmission” categories (Fig. 3C, Dataset S6). Finally, intergenic regions showed enriched annotations about synapse regulation, transmission and plasticity (Fig. 3D, Dataset S7).

Data crossing revealed that H3K9-bhb was present in 547 promoter regions and 681 enhancers common to brain and liver (Dataset S8). KEGG pathway analysis highlighted several enriched annotations related to metabolism for the common enhancers, among them “Insulin signaling”, “mTOR signaling”, “FOXO signaling” pathway, and “circadian entrainment” and “circadian rhythms” (Dataset S9). “FOXO signaling” pathway was present also in the common promoter list (Dataset S10).

Overall, these data demonstrate that 48h fasting is able to remodel the neural chromatin landscape, inducing a dynamic and robust H3K9-bhb in the cerebral cortex, preferentially targeting enhancers, promoters and intergenic regions.

H3K9-bhb is linked to active gene expression in neural tissue

To investigate the impact of H3K9-bhb on gene expression in the cortex, we performed an RNA-seq experiment using the same visual cortical samples used for the ChIP-seq experiment. Fasting dramatically remodeled the transcriptome of the cortex altering the expression of 955 transcripts (Benjamini-Hochberg <0.01. For the complete gene list see Dataset S11).

In particular, 341 genes were upregulated and 614 genes were downregulated in F mice (Fig. 4A). The effect was highly consistent in the different samples, as shown by the heatmap obtained from every biological replicate (Fig. 4A). The most overrepresented KEGG pathways among the genes downregulated in fasting were “steroid biosynthesis”, “protein processing in endoplasmic reticulum”, “metabolic pathway”, “purine metabolism” etc. (Fig. 4B, Dataset S12A); categories mainly related to metabolism, thus suggesting the existence of a brain adaptive response to conserve energy. KEGG pathways characterizing the UP in fasting transcripts were “serotonergic synapses”, “oxytocin signaling pathway”, “p53 signaling pathway” (Fig. 4B, Dataset S12B). Notably, The most significant KEGG pathway in the genes upregulated in the neocortex after fasting was “circadian rhythms" (Fig 4B); this is of interest since core-clock genes have been involved in the control of critical period onset in the mouse visual cortex (21). Finally, the interaction network of the 955 differentially expressed genes revealed a variety of interactomes including: “Fox-O” “mTOR” “Insulin” and “PPAR” signaling pathway which are well-known biochemical cascades influenced by fasting; “Glycosaminoglycan metabolism” “Chondroitin sulfate metabolism and biosynthesis” which are components of the perineuronal nets, important for ocular dominance plasticity and critical period timing (22); and again “circadian rhythms” (Fig. S3; for a complete list see Dataset S13).
Finally, gene set enrichment analysis on the whole RNA-seq data set using CAMERA (23) confirmed that “circadian rhythms” is significantly enriched in both GO and KEGG ontologies (Fig. S4A-B). Intriguingly, the reactome pathway displayed a relationship between “circadian rhythms” terms and a variety of proteins related to epigenetic remodeling (Fig. 4C), suggesting that an interplay between circadian and epigenetic mechanisms could be responsible for the brain adaptive response to prolonged fasting.

To understand the role played by H3K9-bhb on the cerebral cortex transcriptome, we crossed our RNA-seq and ChIP-seq data. We found a significant positive correlation between differential H3K9-bhb peaks (F vs AL) and the fold change of the genes upregulated in F (Fig. 5A, all the genes of the RNA-seq up in fasting, Spearman correlation: rho = 0.13, p value = 4.4E-16. Fig. 5B, only genes up in fasting with p value < 0.05, Spearman correlation: rho = 0.19, p value = 6.7E-09). Furthermore, the expression of genes in proximity of loci differentially enriched in H3K9-bhb peaks was selectively upregulated by fasting with respect to all expressed genes (Fig. 5B, Mann-Whitney test : U = 19670177, p < 0.0001). It is worth noting that there was no significant correlation between the differential H3K9-bhb peaks and the genes upregulated in AL condition (Fig. 5C, all the genes of the RNA-seq up in AL, Spearman correlation: rho = 0.0008,

p value = 0.96. Fig. 5C only genes up in AL with p value < 0.05, Spearman correlation: rho = -0.02, p value = 0.41). These results suggest that H3K9-bhb could be related to fasting-induced gene expression in the cerebral cortex of mice.

To gain a better insight on the transcriptional regulatory role of cortical K-bhb after 48h fasting, we analyzed the list of differential and significantly enriched H3K9-bhb DNA loci (Dataset S4) separately considering promoters and enhancers, and crossed them with the correspondent gene levels obtained through the RNA-seq. Indeed, promoters and enhancers are key elements for controlling transcripts' levels, and they were especially influenced by H3K9-bhb in F mice (Fig. 3A). We found a significant correlation between promoters hits and transcripts upregulated in fasting (Fig. 5C, all the genes of the RNA-seq up in fasting, Spearman correlation: rho = 0.17, p value = 5.4E-08. Fig. 5D, only genes up in fasting with p value < 0.05, Spearman correlation: rho = 0.32, p value = 1.2E-07). The genes clustered in the "FoxO signalling pathway" (Fig. 5D). Moreover, GO analysis of the term "Biological process", showed a variety of annotations principally related to transcriptional regulation and PTMs (Dataset S14).

The correlation of RNA-seq genes with H3K9-bhb enhancers gave again a positive value (Fig. 5E, all the genes of the RNA-seq up in fasting, Spearman correlation: rho = 0.09, p value = 0.01). Interestingly, pathways and terms concerning "circadian rhythms" came up both in the KEGG (Fig 5E and Dataset S15) analysis and GO annotation (Dataset S15). Furthermore, GO biological processes related to "chromatin remodeling and modifications" were significant terms. Again and in keeping with the above analysis, we observed the presence of a signature specifically related to circadian clock and epigenetic mechanism, strongly suggesting that those could be the molecular underpinning underlying the cerebral cortex adaptation to a fasting challenge (Fig. 5E).

H3K9-bhb was particularly abundant in intergenic regions in the brain (Fig. 3A). Epigenetic marks present in intergenic regions in the brain have been shown to be sensitive to changes in neuronal activity, such as DNA methylation (24). Fasting-driven changes in H3K9-bhb in intergenic regions positively correlated with the expression of correspondent transcripts upregulated in fasting (Fig. 5F, only genes up in fasting with p value < 0.05, Spearman correlation: rho = 0.16, p value = 0.02). GO biological processes analysis revealed that the H3K9-bhb enriched intergenic regions associated with genes involved in regulation of transcription, chromatin modifications, synaptic plasticity and neurodevelopment (Fig. 5F).

H3K9-bhb influence diurnal gene expression of core-clock genes in the visual cortex of young mice

Protein synthesis regulation and circadian rhythms are important mechanisms in neural function and plasticity (25, 26). Since GO categories associated with these mechanisms consistently emerged in our RNA-seq and ChIP-seq data, we selected these two pathways for in depth analysis of fasting regulation. First, we studied the "insulin and mTOR pathways" by assessing two key signaling steps: serine 235-36 phosphorylation of S6 (Fig. S5A) and Serine 473 phosphorylation of AKT (Fig. S5B). Confirming the hypothesis indicated by the RNA- and ChIP-seq data, both PTMs were significantly reduced in fasting mice, suggesting that protein synthesis could be altered in the cerebral cortex of F mice. Second, we studied "Circadian rhythms", a process representing one of the top hits in the RNA-seq data (Fig. 4B) and in the differential ChIP-seq enhancer analysis (Fig. 5E). We analyzed the expression of core-clock genes in the visual cortex of F and AL mice at 4 different time points (Zeitgeber time (ZT)) every 6 hours throughout the daily cycle (Fig. 6A). The results demonstrated that several clock genes related to transcriptional inhibition, *Per1, Cry1, Cry2*, and *Reverb-a* displayed similar changes in their diurnal profile upon fasting, and were significantly upregulated at ZT4 in F with respect to AL mice, validating the RNA-seq result which was performed at this ZT (Fig. 6B). *Bmal1*, *Clock* and *Ror-a*, belonging to the transcriptional activation limb of the core-clock machinery, were not significantly altered at any ZT in F mice (Fig. 6C), suggesting a certain degree of specificity of fasting effects on the inhibitory limb of the clock machinery.

DISCUSSION

Metabolic influence on the brain has been observed for years, however little is known about the molecular mechanisms activated by metabolic stimuli in brain tissue. In particular caloric restriction or intermittent fasting have been found to ameliorate brain resilience to aging processes (27), but its biochemical and transcriptional consequences on brain tissue in vivo are poorly understood. BHB, a metabolic fuel for the brain mainly produced by the liver during fasting, has been shown to be beneficial in models of neurological diseases (28), epilepsy (29) and stroke (30). These effects have been attributed to BDNF (31, 32), HCAR2 (33), promotion of SIRT3 function (34). However our study shows that a surprisingly high number of proteins can undergo K-bhb, raising the possibility that multiple unknown pathways can mediate BHB effects in the brain with potential therapeutic implications for brain disorders. To our knowledge, this is the first proteome-wide report of beta-hydroxybutyrylation. Interestingly, the proteins

displaying K-bhb belonged to specific GO categories which included regulation of transcription and chromatin modifications, suggesting the tempting possibility of a cross-talk among beta-hydroxybutyrilation and other epigenetic mechanisms in the brain. Further studies are needed to investigate the BHB action on specific proteins and in the distinct cell types composing the neural tissue.

Our work also reveals a conspicuous transcriptomic change induced by fasting in cerebrocortical tissue, and demonstrates that BHB is an epigenetic molecule capable of dramatically remodelling the neural tissue chromatin landscape by post-translationally modifying the histone H3. Fasting induced transcriptional changes and the enrichment of H3K9-bhb on a genome wide scale were significantly correlated suggesting a regulatory role for H3K9-bhb in the neural tissue. Previous work studied H3K9-bhb response to the same fasting duration used here on hepatic tissue (19). Our ChIP-seq analysis in cerebrocortical tissue revealed a number of DNA loci displaying differential H3K9-bhb after fasting summing up to about half of the DNA loci regulated in the liver, indicating that histone beta-hydroxybutyrylation may be a more pervasive PTM in liver than in neural tissue. Importantly, the data crossing of liver and cortex H3K9-bhb ChIP-seq data indicated several common promoters and enhancers among the two tissues. The KEGG pathway of the common enhancers were associated with “circadian rhythms” terms. The effects of fasting on the liver clock are well-known (35, 36), as well as the effects of H3K9-bhb on core-clock gene expression (19). However, how food deprivation could impinge on the cerebral cortex clock is still obscure. Our transcriptome and ChIP-seq data converge into a possible involvement of circadian processes in the brain response to a prolonged fasting (see below).

Based on genomic localization analysis, H3K9-bhb was mainly enriched in the cerebral cortex intergenic, enhancer and promoter regions of fasting mice. The genes neighboring those regions were positively correlated with the RNA-seq results of genes UP in fasting, extending and confirming previous findings in the liver (19), and suggesting that H3K9-bhb is a new PTM linked to active gene expression also in the brain. Although our understanding of intergenic regions function in the brain is still limited, H3K9-bhb in these genomic loci might help regulate the expression of associated transcribed regions, as already observed for DNA methylation in the human brain (37).

The functional annotation analysis of transcriptome, beta-hydroxybutyrylome and epigenome suggest that fasting could impinge on specific pathways, which could cooperate in setting up the best response of brain cells to a condition of scarce access to food. In particular, “circadian

rhythms" is the most significantly enriched KEGG pathway among the upregulated genes, and "circadian entrainment", "circadian regulation of gene expression", "rhythmic process", and again "circadian rhythms", come up in the ChIP-seq functional annotation analysis of enhancer and promoter regions. Thus, diurnal rhythms seem to represent biological processes particularly impacted by fasting in the cerebral cortex. The circadian clock is an inner oscillator system which ensures appropriate physiology and fitness to a variety of organisms (38). Changes in core-clock gene expression after 48h fasting might help to optimize the energetic cycle in neuronal cells, which consume much energy for electrical transmission and membrane potential maintenance; and/or non neuronal cells, which need adequate fuel for surveillance/defense function (e.g.microglia), metabolism, throphism, and secretion/absorption of neurotransmitters etc. (e.g. astrocytes). Intriguingly, our reactome analysis of the cortical transcriptome displayed the existence of a link between circadian rhythms related genes and epigenetic related transcripts (Fig. 4C). Epigenetic mechanisms participate in the formation of circadian oscillation of gene expression, intricately regulating the core-clock machinery (39). The fasting challenge could directly control core-clock gene expression through a complex network of epigenetic proteins, possibly, fine tuning H3K9-bhb and other histone PTM. Furthermore, the circadian clock controls the onset of critical period plasticity in the visual cortex (21). Thus, we might speculate that the molecular/epigenetic/metabolic changes driven by fasting could contribute to alter the plasticity potential of the neural circuits through modulation of the endogenous 24h oscillator. An effect of fasting on plasticity is also in line with the modulation of protein synthesis, a regulatory mechanism involved in plasticity mechanisms (40). This hypothesis will be tested in future experiments.

"Oxytocin signalling" and "serotonergic synapses" are categories present in our transcriptome functional annotation, and they seem particularly relevant for brain function. Oxytocin and serotonin are neuromodulators involved in human affects and socialization (41). For instance they have been shown to be implicated in ASD and depression (42, 43). Prolonged fasting could promote social behaviour in order to cooperate and increase the probability to survive during periods of food scarcity (44). Based on our GO results, intermittent fasting, caloric restriction, KD or ketone supplements might be alternative strategies or adjuvant to traditional treatments for ASD, depression or other neuropsychiatric diseases. This is an intriguing hypothesis which needs further validation in preclinical models to rationalize the use of nutrition to improve brain disorders, and cognitive function in general.

In summary, our work shows that metabolic stimuli are powerful regulators of the transcriptional status of neural tissue modifying the chromatin epigenetic landscape. The regulated genes are not only involved in brain tissue metabolism, but they also include pathways relevant for synaptic transmission and plasticity, raising the hypothesis that the metabolic status of the individual might exert an important regulation on brain function.

FIGURE LEGENDS

Figure 1. Fasting affects blood glucose concentration and locomotor activity

(**a**) Experimental timeline. (**b**) Blood glucose concentration (mg/dL) before and after 48h fasting (AL N=9, F N=10, two-way RM ANOVA time*treatment, interaction $F_{1,17}$=64.19 p<0.0001, post-hoc Sidak, AL vs F (postFASTING) t_{34}=9.203 p<0.0001); (**c**) Weight change (%) before and after 48h fasting (N=10 AL, N=14 F, unpaired 2-tailed t-test, t_{22}=18.06 p<0.0001); (**d**) Spontaneous locomotor activity throughout the daily cycle before and during fasting (N=10 AL, N=7 F, two-way RM ANOVA time*treatment, interaction $F_{5,75}$=6.596 p<0.0001).White and black squares on the x axes represent day-time and night-time respectively.
Error bars represent SEM.

Figure 2. Fasting increases protein Lysine beta-hydroxybutyrylation and modifies the beta-hydroxybutyrylation profile of the total proteome in the cerebral cortex.
(**a**) Western blot analysis of total lysine beta-hydroxybutyrylation in the occipital cortex of F or AL mice using a Pan-K-bhb antibody (top panel), a control beta-tubulin antibody (middle panel) and the Ponceau staining (bottom panel). (**b**) Left: Venn diagram of K-bhb proteins from the occipital cortex of AL (blue) and F mice (red). In purple the K-bhb proteins found in both conditions. Right: GO analysis (biological processes) of K-bhb proteins found in AL, F and in both groups (AL N= 3,F N= 3). (**c**) Western blot analysis of histone lysine beta-hydroxybutirylation in the occipital cortex of F or AL using a specific H3K9-bhb antibody (top panel) or a control H3 antibody (middle panel). Histograms representing the normalized ratio of H3K9-bhb /H3 in F condition compared to AL (AL N=4, F N=4, unpaired 2-tailed t-test, t_6=9.361 p<0.0001).
Error bars represent SEM.

Figure 3. Fasting induces robust changes in H3K9 beta-hydroxybutyrylation in the mouse cerebral cortex.
(**a**) Pie chart of genome-wide distribution of H3K9-bhb enriched loci in F with respect to AL (Cyber-Tp<0.05). (**b**) GO Biological processes (right graph) and KEGG pathway (left graph) analysis of the genes in proximity of promoters. (**c**) Same as b for enhancer regions. (**d**) Same as b for introns. No significant KEGG pathway was found for gene introns.

Figure 4. Fasting is related to active gene expression in the cortex of young mice.

(a) Left: Heat map of RNA-seq analysis performed in the occipital cortex of F and AL mice (AL N=4, F N=4, p<0.05). Right :Venn diagrams representing the differential expressed genes (DEGs) between AL and F in the RNA-seq dataset (n=4, Benjamini-hochberg<0.01). (**b**) KEGG pathways analysis of DEGs in the occipital cortex of F mice. Upper panel : KEGG analysis of DEGs downregulated in the F condition. Lower panel : KEGG analysis of DEGs upregulated in the F condition. (**c**) Reactome pathway of DEG enriched in "circadian rhythms" annotation. Colors: Log2FC. Circle dimensions: Fasting means.

Figure 5. H3K9-bhb is linked to active gene expression in the cortex of fasted mice.

(**a)** Correlation between F-induced H3K9-bhb peak enrichment and transcript fold change revealed by RNA-seq (F vs AL, all the genes of the RNA-seq up in fasting, Spearman correlation: rho = 0.13, p value = 4.4E-16; only genes up in fasting with p value < 0.05, Spearman correlation: rho = 0.19, p value = 6.7E-09). (**b**) fold change expression induced by fasting is significantly higher for genes in proximity of H3K9-bhb peaks than for all genes. Horizontal bar represents median, Mann-Whitney test : U = 19670177, p < 0.0001. (**c**) Lack of correlation between AL-induced H3K9-bhb peak enrichment and transcript fold changes revealed by RNA-seq (all the genes of the RNA-seq up in AL, Spearman correlation: rho = 0.0008, p = 0.96; only genes up in AL with p < 0.05, Spearman correlation: rho = -0.02, p = 0.41). (**d**) Top: Correlation between H3K9-bhb enrichment on promoters and transcript fold-change for genes upregulated in fasting (all the genes of the RNA-seq up in fasting, Spearman correlation: rho = 0.17, p = 5.4E-08; only genes up in fasting with p value < 0.05, Spearman correlation: rho = 0.32, p = 1.2E-07). Bottom: KEGG pathways analysis and GO analysis of the H3K9-bhb promoters of genes upregulated in the fasting condition. (**e**) Top: Correlation between H3K9-bhb enrichment on enhancers and transcript fold-change for genes upregulated in fasting (all the genes of the RNA-seq up in fasting, Spearman correlation: rho = 0.09, p = 0.01). Bottom: KEGG pathways analysis and GO analysis of the H3K9-bhb enhancers of genes upregulated in fasting condition. (**f**) Top: Correlation between H3K9-bhb enriched intergenic regions and transcripts upregulated in fasting (only genes up in fasting with p < 0.05, Spearman correlation: rho = 0.16, p = 0.02).

Figure 6. H3K9-bhb influences the expression of core-clock genes in the cortex of mice. (**a**) Experimental timeline. (**b**) Quantitative real-time PCR analysis of genes related to transcriptional inhibition of the clock core machinery (N=4 per condition, per time-point. Per1 :, two-way ANOVA time*treatment, interaction $F_{3,24}$=3.234 p=0.04, post-hoc Sidak, AL vs F (ZT4) t_{24}=3.209 p=0.015; Cry1: two-way ANOVA time*treatment, interaction $F_{3,24}$=4.836 p=0.009, post-hoc Sidak, AL vs F (ZT4) t_{24}=3.317 p=0.0115; Cry2: F, two-way ANOVA time*treatment, interaction $F_{3,24}$=3.717 p=0.0251, post-hoc Sidak, AL vs F (ZT4) t_{24}=2.999 p=0.0247, (ZT22) t_{24}=2.769 p=0.042; Reverb-a, two-way ANOVA time*treatment, interaction $F_{3,24}$=4.162 p=0.0165, post-hoc Sidak, AL vs F (ZT4) t_{24}=3.144 p=0.0175). (**c**) Quantitative real-time PCR analysis of genes related to transcriptional activation limb of the core clock machinery (N=4 per condition, per time-point. Bmal1: F, two-way ANOVA time*treatment, interaction $F_{3,24}$=1.167 p=0.1804; Clock: two-way RM ANOVA time*treatment, interaction $F_{3,24}$=0.94 p=0.436; RORa: F, two-way RM ANOVA time*treatment, interaction $F_{3,24}$=1.635 p=0.3869).

ACKNOWLEDGMENTS

We thank Manuel Tongiani and Martina Nasisi for their help with the experiments. Special thanks to Elena Putignano (Institute of Neuroscience, CNR), Vania Liverani and Antonella Calvello (Scuola Normale Superiore) for technical assistance in the lab. We thank Prof. Concetta Morrone and Prof. Paola Binda (University of Pisa) for their insightful comments.

This research was supported by H2020-MSCA-IF-2016 749697 GaMePLAY and PRIN2017 2017HMH8FA. The work of SC, MS, CM, and PB was in part supported by NIH grant GM123558 to PB.

Competing Interest Statement

The authors declare no conflict of interest.

Author Contributions

SCo and LL performed all the experiments and analysed the data. SCo prepared the figures. SCh performed the ChIP-seq and RNA-seq analysis. FF and SR performed the Beta-hydroxybutyrilome analysis. MS performed the RNA seq analysis. FR helped with GO analysis. RM helped with correlations between ChIP-seq and RNA-seq. CM helped with ChIP-seq data

alignment and analysis. PB supervised the RNA-seq and ChiP-seq data analysis. PT conceived the project and performed the experiments. TP and PT supervised the project and wrote the manuscript.

MATERIALS AND METHODS

Animals and housing

All experiments were carried out in accordance with the European Directives (2010/63/EU), and were approved by the Italian Ministry of Health (authorization number 354/2020-PR).
C57BL/6J mice were used in this study. Mice were housed in conventional cages (365 x 207 x 140 mm, 2-3 animals per cage) with nesting material. Mice were kept under a 12 hour dark: 12 hour light cycle, with food (standard diet mucedola 4RF25) and water ad libitum.
Mice were weaned at postnatal day (P) 21. At P33 a group of mice were subjected to complete fasting (F group) for 2 days, until P35, through removal of the food from the cage and ad libitum access to water. Age-matched control mice (AL group) continued to have ad libitum access to food and water. After two days, mice were sacrificed by decapitation. Liver and occipital cortices (corresponding to the visual cortex) were harvested, snapped frozen in liquid nitrogen and stored at -80 until use. For the day vs night sample analysis mice were sacrificed every 6 hours along the diurnal cycle (from ZT0 to ZT24). For every group of mice the food was precisely removed 48 hours before the ZT of the sacrifice.

Spontaneous locomotor activity

Opto M3 multi-channel activity monitors (Columbus Instruments, OH, USA) were used to quantify spontaneous locomotor activity of animals. Monitors were placed in the colony area and testing was conducted in the same conditions of animal facility housing. All measurements were performed from 6:00 P.M. to 6:00 A.M. (dark phase) and to 6:00 A.M. to 6:00 P.M. (light phase). Individual mice were placed in 33 × 15 × 13-cm (length × width × height) clear plastic cages and total distance travelled was calculated from infrared beam breaks by determining activity at 1-min intervals. Horizontal activity was measured by the sequential breaking of infrared beams, 2.54 cm on center, in the horizontal plane of the x axis.

RNA extraction

Cortex samples were homogenized in Phenol/guanidine-based QIAzol Lysis Reagent (Qiagen #79306). Chloroform was added and the samples were shacked for 15 s. The samples were left at 20–24°C for 3 min and then centrifuged (12000*xg*, 20 min, 4 °C). The upper phase aqueous solution, containing RNA, was collected in a fresh tube and the RNA was precipitated by the addition of isopropanol. Samples were mixed by vortexing, left at RT for 10 min and then

centrifuged (12000*xg*, 15 min, 4 °C). Supernatant was discarded and the RNA pellet was washed in 75% ethanol by centrifugation (7500*xg*, 5 min, 4 °C). Supernatant was discarded and the pellet was left to dry for at least 15 min; then, it was resuspended in RNAse free water. RNA concentration was determined by Nanodrop Spectrophotometer (Thermoscientific 2000 C). RNA quality was analyzed through a gel running (1% agarose). Total RNA was reverse transcribed using QuantiTech Reverse Transcription Kit (Qiagen # 205311).

Gene expression was analyzed by real-time PCR (Step one, Applied Biosystems), using PowerUp SYBR Green Master Mix (Thermo Fisher #A25742). The primers for gene expression were designed by Primer 3 software (v. 0.4.0) and reported in the following table:

Primer Table

mBmal1 FOR	5' GCAGTGCCACTGACTACCAAGA 3'
mBmal1 REV	5' TCCTGGACATTGCATTGCAT 3'
mCry2 FOR	5' CAACACAGGCCCCAGAGCACTATC 3'
mCry2 REV	5' TCAGGAGTCCTTGCTTGCTGGCTC 3'
mCry1 FOR	5’ CAGACTCACTCACTCAAGCAAGG 3’
mCry1 REV	5’ TCAGTTACTGCTCTGCCGCTGGAC 3’
mReverb-a FOR	5' AGGCTGCTCAGTTGGTTGTT 3'
mReverb-a REV	5' CTCCATCGTTCGCATCAATC 3'
mPer1 FOR	5’ ACCAGCGTGTCATGATGACATA 3’
mPer1 REV	5’ GTGCACAGCACCCAGTTCCC 3’
mRor-a FOR	5' ACCGTGTCCATGGCAGAAC 3'
mRor-a REV	5' TTTCCAGGTGGGATTTGGAT 3'
mClock FOR	5' ACCACAGCAACAGCAACAAC 3'
mClock REV	5' GGCTGCTGAACTGAAGGAAG 3'

Quantitative values for cDNA amplification were calculated from the threshold cycle number (Ct) obtained during the exponential growth of the PCR products. Threshold was set automatically by the Step one software. Data were analyzed by the ΔΔCt methods using 18S rRNA to normalize the cDNA levels of the transcripts under investigation.

RNA sequencing and data analysis

N=4 biological replicates per experimental group were used in the RNA-seq experiment. Total RNA was extracted as described above, libraries prepared and sequenced on Illumina HiSeq2500 instrument during a pair-end read 125bp sequencing, producing sequencing results in FastQ format. The FastQ files were processed through the standard Tuxedo protocol, using Tophat and Cufflinks. Tophat was used to align the RNA-seq reads to the reference genome assembly mm10 and Cufflinks was used to calculate gene expression levels. This protocol outputs the FPKM values for each gene of each replicate. The differential analysis of the FPKM values across all experiment and control groups was conducted with Cyber-T, a differential analysis program using Bayesian-regularized t-test (45, 46). The p-value threshold used for determining differential expression was 0.05 for all groups. The statistic was corrected using the Benjamini-Ochberg (BH) test for significance.

Protein extraction and Western blot

For total protein extracts, liver and cerebral cortex samples were homogenized in modified RIPA buffer (50 mM Tris pH8, 150mM NaCl, 5mm EDTA, 15mM MgCl2, 1% NP40) plus protease inhibitors. The samples were sonicated one minute on ice (10 sec on/10 sec off) and centrifuged for 15 min at 14000g 4°C. The supernatant was recovered and the protein concentration was determined by Bradford assay (Biorad #5000006) using a Nanodrop Spectrophotometer (Thermoscientific 2000 C).

8% SDS-PAGE was performed to check bhb-Lysine, phospho(Ser235-236)S6, total S6, phospho(Ser473)AKT and total AKT levels. 15% SDS-PAGE was performed to analyse H3 and total H3K9-bhb. The samples were blotted onto nitrocellulose membranes (Biorad) and blocked in 5% BSA in Tris-buffered saline (TBS) for 1 hour at room temperature RT. The nitrocellulose membrane was incubated at 4°C overnight with the following antibodies: anti-phospho(Ser235-236)S6 (Cell signalling Technology #2211S) 1:1000, anti-S6 (Cell signalling Technology #2217) 1:1000, and anti-phospho (Ser473) AKT 1:1000 (Cell signalling technology #9271), AKT 1:1000

(Cell signalling technology #9272), bhb-Lysine 1:2000 (PTM Biolabs #1201), H3K9-bhb 1:2000 (PTM Biolabs #1250), H3 1:5000 (Abcam #1791), beta-tubulin 1:3000 (Sigma #T4026). Blots were then washed 3 times in TTBS for thirty minutes, incubated in HRP conjugated anti-mouse or anti-rabbit diluted (1:8000) in 2.5% BSA in TTBS for one hour at RT. The membranes were then rinsed three times in TTBS and incubated in enhanced chemiluminescent substrate (Millipore) and acquired through a Chemidoc XRS instrument. Bands densitometry was analyzed through ImageJ software.

Beta-hydroxybutyrilome analysis

Cerebral cortex samples were homogenized in 50 mM Tris-HCl, 120 mM NaCl, 1% sodium deoxycholate, briefly sonicated on ice, and centrifuge for 15 min at 14000g 4°C. The supernatant was recovered and the protein concentration was determined by Bradford assay (Biorad) using a Nanodrop Spectrophotometer (Thermoscientific 2000 C). For each condition, 50 µg of proteins were reduced with dithiothreitol (10 mM, for 30 min, at 65°C) and alkylated using iodoacetamide (22 mM, 30 min, room temperature) in dark conditions. Protein digestion was performed using trypsin (w/w ratio 1:50) at 37 °C for 16 hours. Samples were incubated with 1% trifluoroacetic acid (Sigma-Aldrich) for 45 min at 37°C to quench trypsin reaction and to remove sodium deoxycholate by acid precipitation. Samples were centrifuged at 16,000 x g for 10 min and subsequently desalted with Mobicol spin columns equipped with 10 µm pore size filters and filled with VersaFlash C18 spherical 70 Å silica particles (Sigma-Aldrich). Peptides were lyophilized and consequently dissolved in 2% acetonitrile / 0.1 formic acid to achieve a final peptide concentration of 1µg/µL before liquid chromatography tandem mass spectrometry (LC-MS/MS) analysis. The equivalent of 5 µg per sample were directly loaded with an Eksigent expert™ microLC 200 system (Eksigent, AB Sciex, Framingham, MA, USA) and acquired using a 5600+ TripleTOF mass spectrometer (AB Sciex). After loading, peptides were separated on a Jupiter 150 x 0.3 mm, 4 µm 90 Å capillary column with a gradient from 2 to 35% buffer B (acetonitrile / 0.1 formic acid) in 40 min at a flow rate of 5 µL/min. LC column was directly interfaced with a DuoSpray™ ESI ion source operating at 5.5 kV for peptide ionization. Samples were analyzed with an information dependent acquisition (IDA) tandem mass spectrometry method based on a MS1 survey scan from which the 20 most abundant precursor ions were selected for subsequent CID fragmentation to generate MS2 spectra. MS1 survey and MS2 scans were acquired with a resolving power of 30000 and 25000 and over a mass range of 250 – 1250 m/z and 150 -1500 m/z, respectively. Isolation width for precursor ion selection was set at 0.7 m/z on a Q1. The accumulation time was set to 250 milliseconds for MS1 scans while 100

milliseconds for MS2 scans. Charge states of 1+ were excluded from ion selection. Rolling collision energy with a collision energy spread across 5 eV and background subtraction were enabled to achieve the optimal fragmentation according to m/z ratio and charge state and to increase sensitivity. Peak areas of peptides associated to unique proteins were summed together to achieve total protein abundance values that were normalized through the total ion current (TIC) extracted from the full MS1 survey scan acquisition for each run. Proteins were considered to be significantly different with a p-value lower than 0.05 and a fold change (|FC|) > 1.5.

Chromatin Immunoprecipitation (ChIP)

Minced frozen cortices were crosslinked with 1% formaldehyde for 10 min followed by Glycine (0.125M final concentration) at room temperature for 10 min. After homogenizing tissue pellets in PBS, 1 ml of lysis buffer was added. Samples were sonicated by Bioruptor (15 cycles, every cycle: 30 sec ON / 30 sec OFF, power high) to generate 200-500 base pairs fragments and centrifuged at 14000g at 4^{o}C. Supernatants were diluted in dilution buffer (1.1% Triton X100, 1.2 mM EDTA, 16.7 mM Tris-HCl, 167 mM NaCl), and incubated with the following primary antibody 3ug H3K9bhb (PTM Biolab #1250) overnight at 4^{o}C. To monitor the specificity of ChIP assays, samples were also immunoprecipitated with a specific-antibody isotype matched control immunoglobulin (IgG). Protein-G beads (Invitrogen #10004D) were added to the supernatant and incubated for 2 hrs at 4^{o}C and centrifuged. Beads were recovered, washed in low salt buffer, high salt buffer, LiCl buffer, followed by washing in TE for three times. Elution buffer (300 mM NaCl, 0.5% SDS, 10 mM Tris-HCl, 5mM EDTA) was added to the washed beads, treated with RNase at 37^{o}C for 2 hrs and Proteinase K at 65^{o}C overnight. Equal amount of Phenol-Chloroform-Isoamyl Alcohol was added to the samples and the aqueous phase was recovered. DNA was precipitated by adding 100% Ethanol, NaAc and glycogen and kept at -20^{o}C overnight. Samples were centrifuged at 14000g for 30 min at 4^{o}C and washed with 70% ethanol followed by centrifugation at 14000g for 15 min at 4^{o}C.

ChIP-sequencing and analysis

N=4 biological replicates per experimental group were used for the sequencing. IPs and controls were processed in parallel and libraries were prepared at the institute of Applied Genomics (Udine, Italy). The sequencing was performed on Hiseq2500 in 125 bp paired-end mode. The sequencing reads were aligned to the mouse genome assembly mm10 with Bowtie2. Enriched genome areas, peaks, were identified with the MACS2 algorithm. Peak

annotation was performed with in-house annotating tools. Peaks whose start to end position cover regions including promoter, enhancer, utr3, utr5, exon, intron, 2000 base pair downstream of promoter, or intergenic region were annotated and the percentages of the peak's coverage of those regions were calculated. The closest gene and TSS to each peak were identified and their distances to the peak were calculated.

Gene ontology (GO) terms analysis and Functional network generation

Gene ontology analysis was performed using Database for Annotation, Visualization and Integrated Discovery (DAVID) v6.7, using genomic background; and the Kyoto Encyclopedia of Genes and Genomes (KEGG) pathway and GO Biological Processes were chosen for gene clustering. To confirm the results, the CAMERA approach (23, 34), available through EnrichmentBrowser (47), was also used for gene-set enrichment analysis after gene-ranking based on differential expression log fold changes. Cytoscape 3.7.2 software was used to visualize complex networks of interactions in the data-sets, and integrate them with functional annotations.

Statistical analysis

The majority of statistical analyses were performed using GraphPad Prism version 7 (GraphPad Software, San Diego, CA, USA).

Western blot : Differences between groups were tested for significance using unpaired t-tests.

qPCR: Differences between groups were tested for significance using two-way ANOVA. Holm–Sidak's multiple comparisons *post hoc* tests were performed, when appropriate, to correct for multiple hypothesis testing.

Correlation between RNA-seq and ChIP-seq data-sets: Spearman correlation was run on the datasets. The results were considered significant when p was <.05.

All data are represented as the mean ± SEM unless otherwise stated. N refers to single animals unless otherwise stated. In the figures *p<.05; **p<.001, ***p<.0001. Error bars represent SEM.

Data availability

RNA-seq and ChIP-seq data are available on the GEO database: accession number GSE168725

REFERENCES

1. F. Gómez-Pinilla, Brain foods: the effects of nutrients on brain function. *Nature Reviews Neuroscience* **9**, 568–578 (2008).

2. M. P. Mattson, K. Moehl, N. Ghena, M. Schmaedick, A. Cheng, Intermittent metabolic switching, neuroplasticity and brain health. *Nature Reviews Neuroscience* **19**, 80–80 (2018).

3. P. Tognini, *et al.*, Reshaping circadian metabolism in the suprachiasmatic nucleus and prefrontal cortex by nutritional challenge. *Proc. Natl. Acad. Sci. U. S. A.* **117**, 29904–29913 (2020).

4. J. B. Dixon, *et al.*, Severely obese people with diabetes experience impaired emotional well-being associated with socioeconomic disadvantage: Results from diabetes MILES – Australia. *Diabetes Research and Clinical Practice* **101**, 131–140 (2013).

5. S. Dutheil, K. T. Ota, E. S. Wohleb, K. Rasmussen, R. S. Duman, High-Fat Diet Induced Anxiety and Anhedonia: Impact on Brain Homeostasis and Inflammation. *Neuropsychopharmacology* **41**, 1874–1887 (2016).

6. S. Gillette-Guyonnet, B. Vellas, Caloric restriction and brain function. *Current Opinion in Clinical Nutrition and Metabolic Care* **11**, 686–692 (2008).

7. B. Martin, M. P. Mattson, S. Maudsley, Caloric restriction and intermittent fasting: Two potential diets for successful brain aging. *Ageing Research Reviews* **5**, 332–353 (2006).

8. A. Lutas, G. Yellen, The ketogenic diet: metabolic influences on brain excitability and epilepsy. *Trends Neurosci.* **36**, 32–40 (2013).

9. A. Evangeliou, *et al.*, Application of a Ketogenic Diet in Children With Autistic Behavior: Pilot Study. *Journal of Child Neurology* **18**, 113–118 (2003).

10. E. van der Louw, *et al.*, Ketogenic diet guidelines for infants with refractory epilepsy. *European Journal of Paediatric Neurology* **20**, 798–809 (2016).

11. A. Paoli, A. Rubini, J. S. Volek, K. A. Grimaldi, Beyond weight loss: a review of the therapeutic uses of very-low-carbohydrate (ketogenic) diets. *European Journal of Clinical Nutrition* **67**, 789–796 (2013).

12. J. Lee, W. Duan, M. P. Mattson, Evidence that brain-derived neurotrophic factor is required for basal neurogenesis and mediates, in part, the enhancement of neurogenesis by dietary restriction in the hippocampus of adult mice. *J. Neurochem.* **82**, 1367–1375 (2002).

13. C. Vivar, *et al.*, Monosynaptic inputs to new neurons in the dentate gyrus. *Nat. Commun.* **3**, 1107 (2012).

14. J. C. Newman, E. Verdin, Ketone bodies as signaling metabolites. *Trends Endocrinol. Metab.* **25**, 42–52 (2014).

15. I. Kimura, *et al.*, Short-chain fatty acids and ketones directly regulate sympathetic nervous system via G protein-coupled receptor 41 (GPR41). *Proceedings of the National Academy of Sciences* **108**, 8030–8035 (2011).

16. A. K. P. Taggart, *et al.*, (d)-β-Hydroxybutyrate Inhibits Adipocyte Lipolysis via the Nicotinic Acid Receptor PUMA-G. *Journal of Biological Chemistry* **280**, 26649–26652 (2005).

17. Y.-J. Won, V. B. Lu, H. L. Puhl 3rd, S. R. Ikeda, β-Hydroxybutyrate modulates N-type calcium channels in rat sympathetic neurons by acting as an agonist for the G-protein-coupled receptor FFA3. *J. Neurosci.* **33**, 19314–19325 (2013).

18. T. Shimazu, *et al.*, Suppression of oxidative stress by β-hydroxybutyrate, an endogenous histone deacetylase inhibitor. *Science* **339**, 211–214 (2013).

19. Z. Xie, *et al.*, Metabolic Regulation of Gene Expression by Histone Lysine β-Hydroxybutyrylation. *Mol. Cell* **62**, 194–206 (2016).

20. H. E. Koubi, *et al.*, Fasting-induced rise in locomotor activity in rats coincides with increased protein utilization. *Physiol. Behav.* **50**, 337–343 (1991).

21. Y. Kobayashi, Z. Ye, T. K. Hensch, Clock genes control cortical critical period timing. *Neuron* **86**, 264–275 (2015).

22. T. Pizzorusso, *et al.*, Reactivation of ocular dominance plasticity in the adult visual cortex. *Science* **298**, 1248–1251 (2002).

23. D. Wu, G. K. Smyth, Camera: a competitive gene set test accounting for inter-gene correlation. *Nucleic Acids Research* **40**, e133–e133 (2012).

24. J. U. Guo, *et al.*, Neuronal activity modifies the DNA methylation landscape in the adult brain. *Nat. Neurosci.* **14**, 1345–1351 (2011).

25. K. C. Martin, M. Barad, E. R. Kandel, Local protein synthesis and its role in synapse-specific plasticity. *Curr. Opin. Neurobiol.* **10**, 587–592 (2000).

26. M. J. Hartsock, R. L. Spencer, Memory and the circadian system: Identifying candidate mechanisms by which local clocks in the brain may regulate synaptic plasticity. *Neurosci. Biobehav. Rev.* **118**, 134–162 (2020).

27. L. R. Mujica-Parodi, *et al.*, Diet modulates brain network stability, a biomarker for brain aging, in young adults. *Proc. Natl. Acad. Sci. U. S. A.* **117**, 6170–6177 (2020).

28. H. Yang, W. Shan, F. Zhu, J. Wu, Q. Wang, Ketone Bodies in Neurological Diseases: Focus on Neuroprotection and Underlying Mechanisms. *Front. Neurol.* **10**, 585 (2019).

29. T. A. Simeone, K. A. Simeone, J. M. Rho, Ketone Bodies as Anti-Seizure Agents. *Neurochem. Res.* **42**, 2011–2018 (2017).

30. J. S. Stephan, S. F. Sleiman, Exercise Factors Released by the Liver, Muscle, and Bones Have Promising Therapeutic Potential for Stroke. *Front. Neurol.* **12**, 600365 (2021).

31. S. F. Sleiman, *et al.*, Exercise promotes the expression of brain derived neurotrophic factor (BDNF) through the action of the ketone body β-hydroxybutyrate. *Elife* **5** (2016).

32. L. Chen, Z. Miao, X. Xu, β-hydroxybutyrate alleviates depressive behaviors in mice possibly by increasing the histone3-lysine9-β-hydroxybutyrylation. *Biochem. Biophys. Res. Commun.* **490**, 117–122 (2017).

33. M. Rahman, *et al.*, The β-hydroxybutyrate receptor HCA2 activates a neuroprotective subset of macrophages. *Nature Communications* **5** (2014).

34. J. Yin, P. Han, Z. Tang, Q. Liu, J. Shi, Sirtuin 3 mediates neuroprotection of ketones against ischemic stroke. *J. Cereb. Blood Flow Metab.* **35**, 1783–1789 (2015).

35. C. Vollmers, *et al.*, Time of feeding and the intrinsic circadian clock drive rhythms in hepatic gene expression. *Proc. Natl. Acad. Sci. U. S. A.* **106**, 21453–21458 (2009).

36. K. Kinouchi, *et al.*, Fasting Imparts a Switch to Alternative Daily Pathways in Liver and Muscle. *Cell Rep.* **25**, 3299–3314.e6 (2018).

37. F. Telese, A. Gamliel, D. Skowronska-Krawczyk, I. Garcia-Bassets, M. G. Rosenfeld, "Seq-ing" insights into the epigenetics of neuronal gene regulation. *Neuron* **77**, 606–623 (2013).

38. A. Zarrinpar, A. Chaix, S. Panda, Daily Eating Patterns and Their Impact on Health and Disease. *Trends Endocrinol. Metab.* **27**, 69–83 (2016).

39. K. Eckel-Mahan, P. Sassone-Corsi, Epigenetic regulation of the molecular clockwork. *Prog. Mol. Biol. Transl. Sci.* **119**, 29–50 (2013).

40. I. J. Cajigas, T. Will, E. M. Schuman, Protein homeostasis and synaptic plasticity. *The EMBO Journal* **29**, 2746–2752 (2010).

41. R. Mottolese, J. Redouté, N. Costes, D. Le Bars, A. Sirigu, Switching brain serotonin with oxytocin. *Proc. Natl. Acad. Sci. U. S. A.* **111**, 8637–8642 (2014).

42. H. Yamasue, G. Domes, Oxytocin and Autism Spectrum Disorders. *Behavioral Pharmacology of Neuropeptides: Oxytocin*, 449–465 (2017).

43. D. O. Borroto-Escuela, *et al.*, The Role of Central Serotonin Neurons and 5-HT Heteroreceptor Complexes in the Pathophysiology of Depression: A Historical Perspective and Future Prospects. *Int. J. Mol. Sci.* **22** (2021).

44. O. Weiss, A. Dorfman, T. Ram, P. Zadicario, D. Eilam, Rats do not eat alone in public: Food-deprived rats socialize rather than competing for baits. *PLoS One* **12**, e0173302 (2017).

45. P. Baldi, A. D. Long, A Bayesian framework for the analysis of microarray expression data: regularized t -test and statistical inferences of gene changes. *Bioinformatics* **17**, 509–519 (2001).

46. M. A. Kayala, P. Baldi, Cyber-T web server: differential analysis of high-throughput data. *Nucleic Acids Res.* **40**, W553–9 (2012).

47. L. Geistlinger, G. Csaba, R. Zimmer, Bioconductor's EnrichmentBrowser: seamless navigation through combined results of set- & network-based enrichment analysis. *BMC Bioinformatics* **17**, 45 (2016).

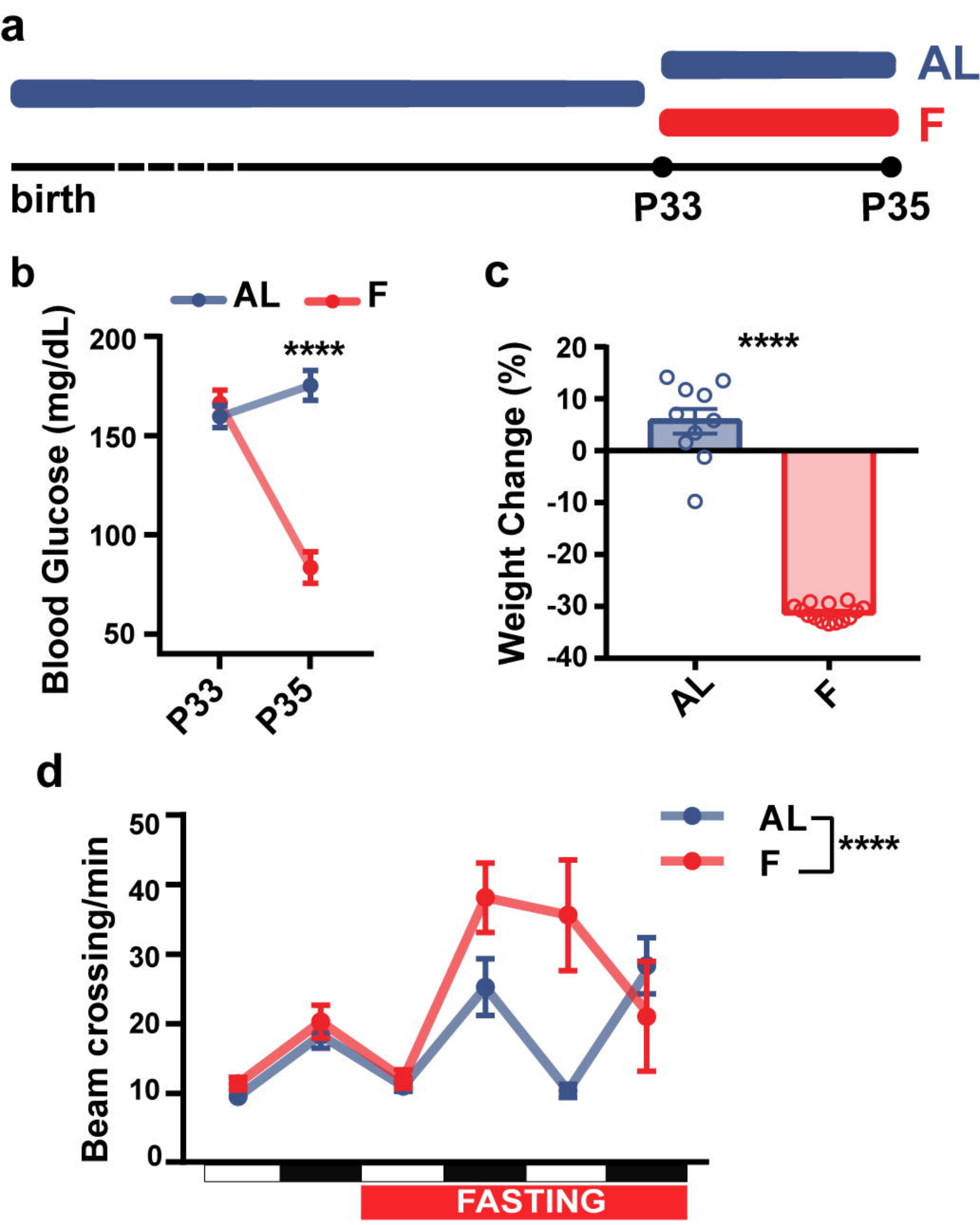
a
AL
F
birth
P33
P35
b
AL
F
Blood Glucose (mg/dL)
200
150
100
50
****
P33
P35
c
Weight Change (%)
20
10
0
-10
-20
-30
-40
****
AL
F
d
Beam crossing/min
50
40
30
20
10
0
AL
F
****
FASTING

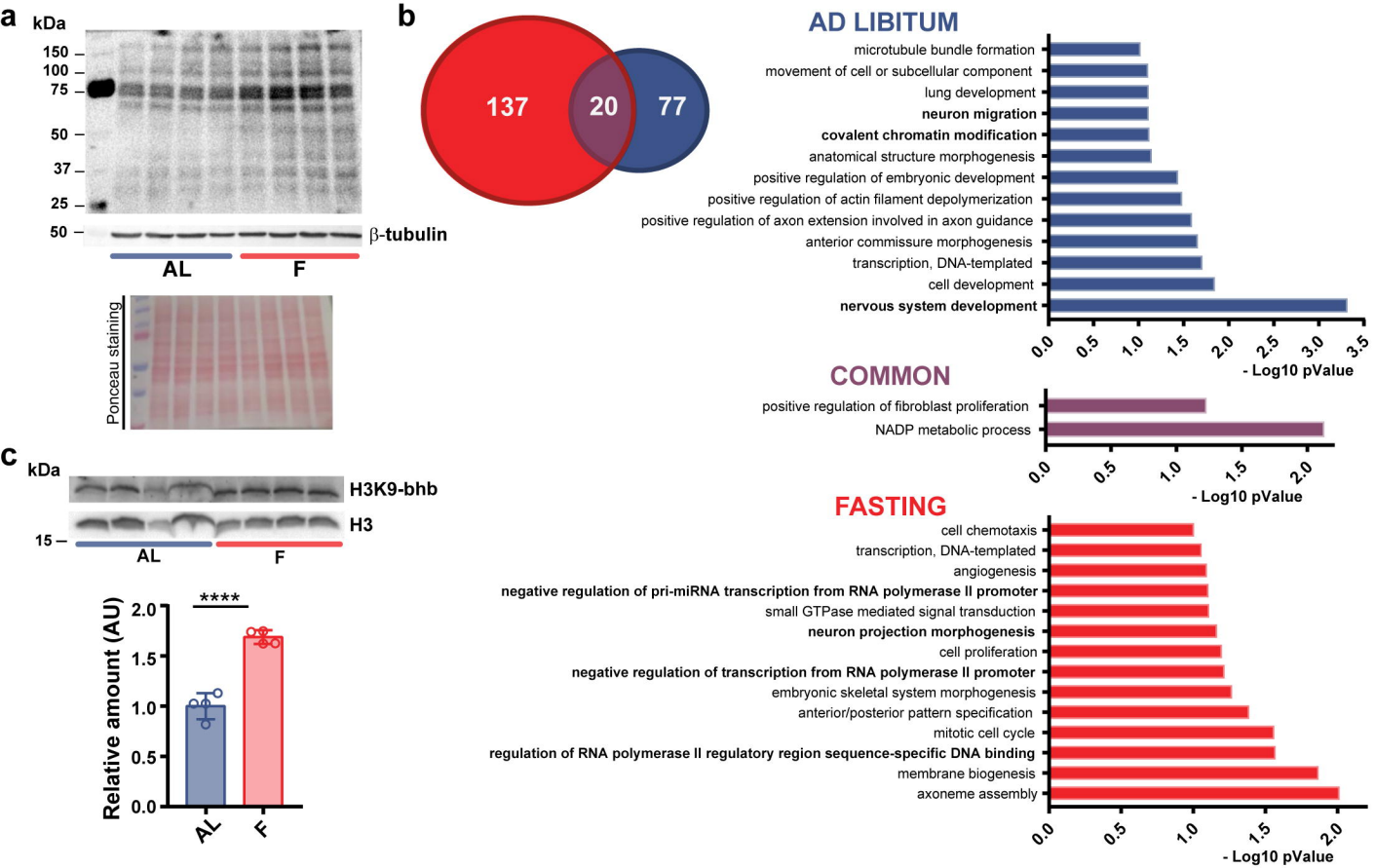
a
kDa
150
100
75
50
37
25
50
β-tubulin
AL
F
Ponceau staining
b
137
20
77
AD LIBITUM
microtubule bundle formation
movement of cell or subcellular component
lung development
neuron migration
covalent chromatin modification
anatomical structure morphogenesis
positive regulation of embryonic development
positive regulation of actin filament depolymerization
positive regulation of axon extension involved in axon guidance
anterior commissure morphogenesis
transcription, DNA-templated
cell development
nervous system development
0.0 0.5 1.0 1.5 2.0 2.5 3.0 3.5
- Log10 pValue
COMMON
positive regulation of fibroblast proliferation
NADP metabolic process
0.0 0.5 1.0 1.5 2.0
- Log10 pValue
FASTING
cell chemotaxis
transcription, DNA-templated
angiogenesis
negative regulation of pri-miRNA transcription from RNA polymerase II promoter
small GTPase mediated signal transduction
neuron projection morphogenesis
cell proliferation
negative regulation of transcription from RNA polymerase II promoter
embryonic skeletal system morphogenesis
anterior/posterior pattern specification
mitotic cell cycle
regulation of RNA polymerase II regulatory region sequence-specific DNA binding
membrane biogenesis
axoneme assembly
0.0 0.5 1.0 1.5 2.0
- Log10 pValue
c
kDa
H3K9-bhb
H3
15
AL
F
****
Relative amount (AU)
2.0
1.5
1.0
0.5
0.0
AL
F

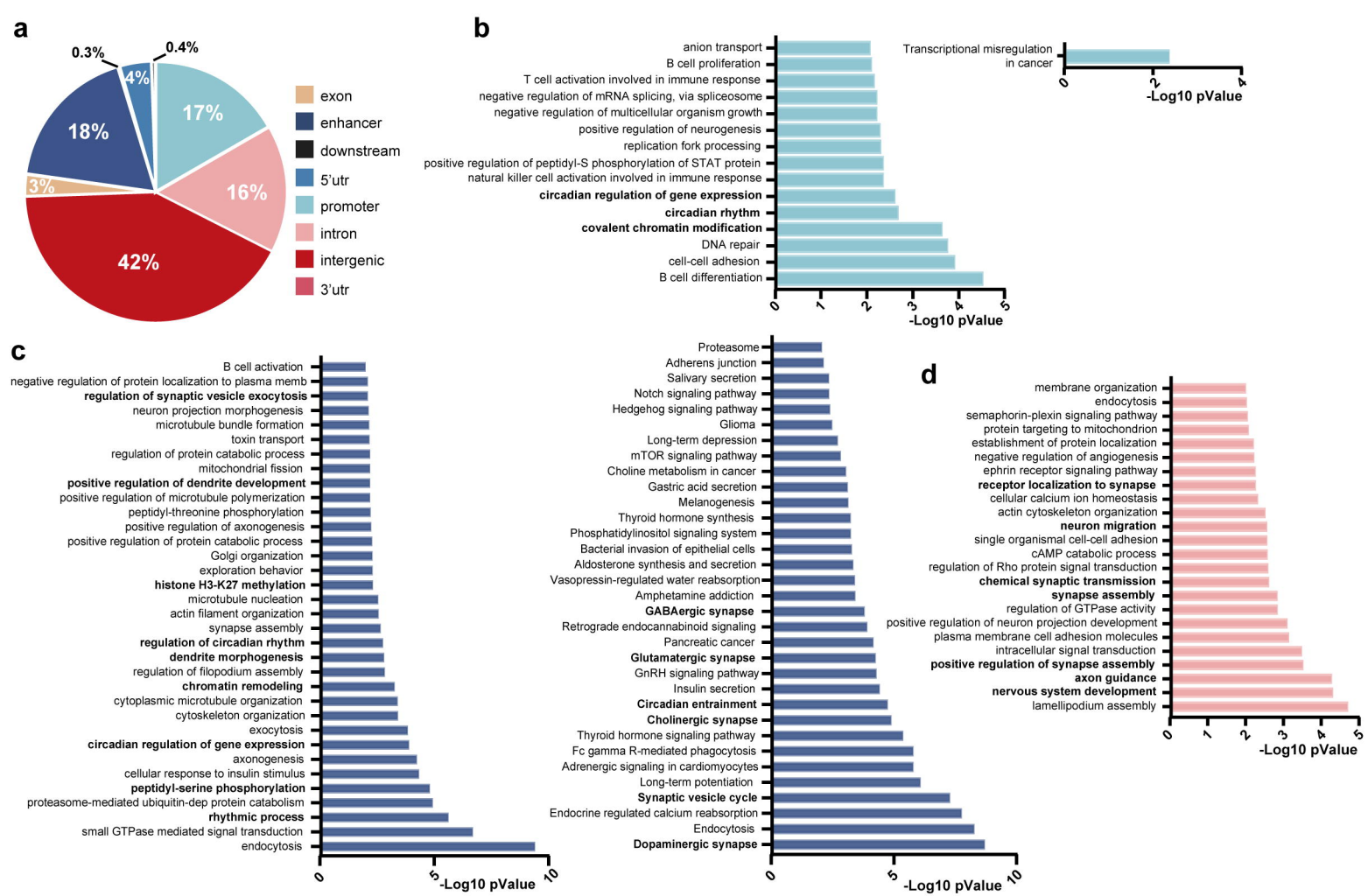
a
0.3%
0.4%
4%
17%
18%
3%
16%
42%
exon
enhancer
downstream
5'utr
promoter
intron
intergenic
3'utr
b
anion transport
B cell proliferation
T cell activation involved in immune response
negative regulation of mRNA splicing, via spliceosome
negative regulation of multicellular organism growth
positive regulation of neurogenesis
replication fork processing
positive regulation of peptidyl-S phosphorylation of STAT protein
natural killer cell activation involved in immune response
circadian regulation of gene expression
circadian rhythm
covalent chromatin modification
DNA repair
cell-cell adhesion
B cell differentiation
0 1 2 3 4 5
-Log10 pValue
Transcriptional misregulation in cancer
0 2 4
-Log10 pValue
c
B cell activation
negative regulation of protein localization to plasma memb
regulation of synaptic vesicle exocytosis
neuron projection morphogenesis
microtubule bundle formation
toxin transport
regulation of protein catabolic process
mitochondrial fission
positive regulation of dendrite development
positive regulation of microtubule polymerization
peptidyl-threonine phosphorylation
positive regulation of axonogenesis
positive regulation of protein catabolic process
Golgi organization
exploration behavior
histone H3-K27 methylation
microtubule nucleation
actin filament organization
synapse assembly
regulation of circadian rhythm
dendrite morphogenesis
regulation of filopodium assembly
chromatin remodeling
cytoplasmic microtubule organization
cytoskeleton organization
exocytosis
circadian regulation of gene expression
axonogenesis
cellular response to insulin stimulus
peptidyl-serine phosphorylation
proteasome-mediated ubiquitin-dep protein catabolism
rhythmic process
small GTPase mediated signal transduction
endocytosis
0 5 10
-Log10 pValue
Proteasome
Adherens junction
Salivary secretion
Notch signaling pathway
Hedgehog signaling pathway
Glioma
Long-term depression
mTOR signaling pathway
Choline metabolism in cancer
Gastric acid secretion
Melanogenesis
Thyroid hormone synthesis
Phosphatidylinositol signaling system
Bacterial invasion of epithelial cells
Aldosterone synthesis and secretion
Vasopressin-regulated water reabsorption
Amphetamine addiction
GABAergic synapse
Retrograde endocannabinoid signaling
Pancreatic cancer
Glutamatergic synapse
GnRH signaling pathway
Insulin secretion
Circadian entrainment
Cholinergic synapse
Thyroid hormone signaling pathway
Fc gamma R-mediated phagocytosis
Adrenergic signaling in cardiomyocytes
Long-term potentiation
Synaptic vesicle cycle
Endocrine regulated calcium reabsorption
Endocytosis
Dopaminergic synapse
0 5 10
-Log10 pValue
d
membrane organization
endocytosis
semaphorin-plexin signaling pathway
protein targeting to mitochondrion
establishment of protein localization
negative regulation of angiogenesis
ephrin receptor signaling pathway
receptor localization to synapse
cellular calcium ion homeostasis
actin cytoskeleton organization
neuron migration
single organismal cell-cell adhesion
cAMP catabolic process
regulation of Rho protein signal transduction
chemical synaptic transmission
synapse assembly
regulation of GTPase activity
positive regulation of neuron projection development
plasma membrane cell adhesion molecules
intracellular signal transduction
positive regulation of synapse assembly
axon guidance
nervous system development
lamellipodium assembly
0 1 2 3 4 5
-Log10 pValue

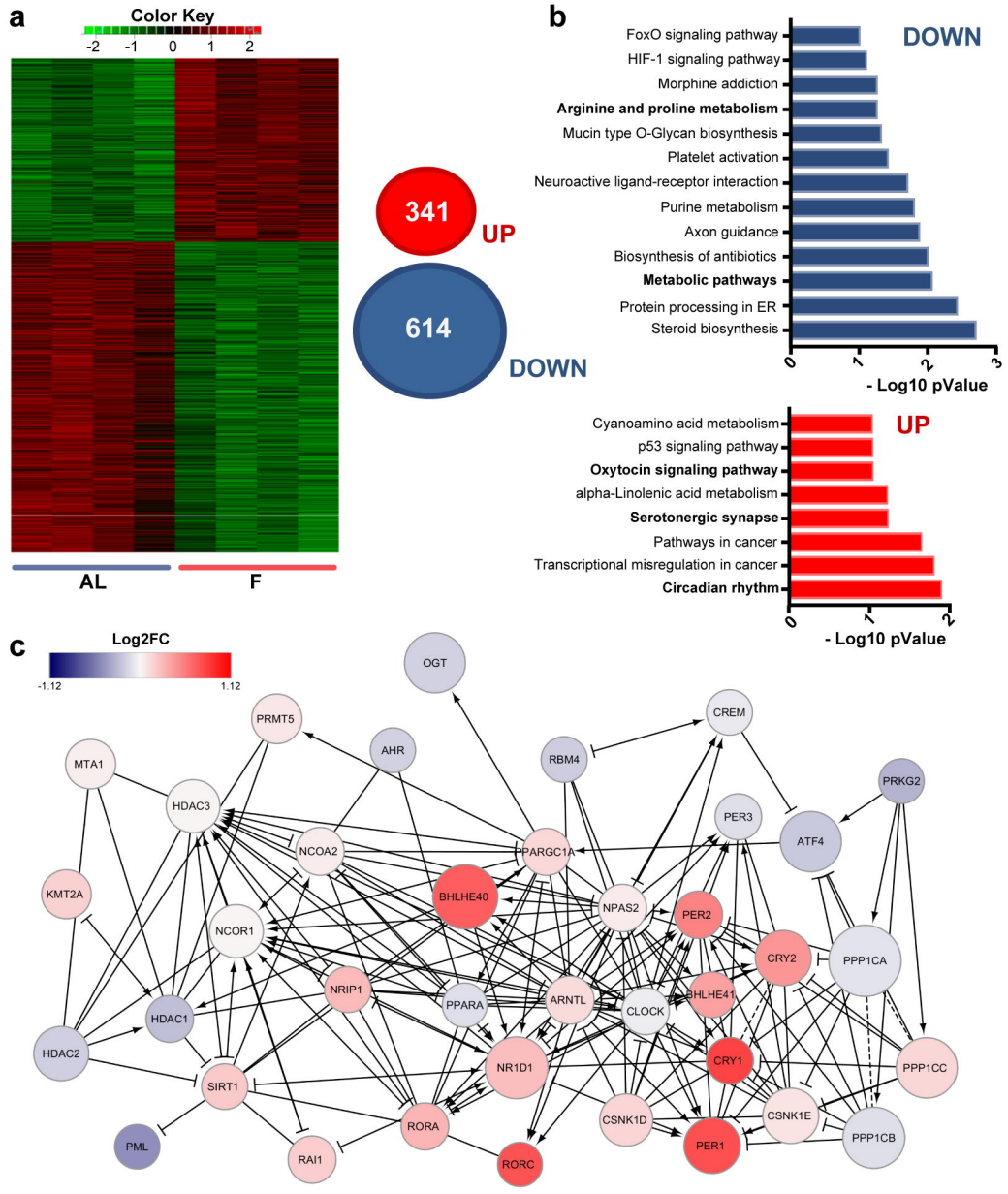
a
Color Key
-2
-1
0
1
2
AL
F
341
UP
614
DOWN
b
DOWN
FoxO signaling pathway
HIF-1 signaling pathway
Morphine addiction
Arginine and proline metabolism
Mucin type O-Glycan biosynthesis
Platelet activation
Neuroactive ligand-receptor interaction
Purine metabolism
Axon guidance
Biosynthesis of antibiotics
Metabolic pathways
Protein processing in ER
Steroid biosynthesis
0
1
2
3
- Log10 pValue
UP
Cyanoamino acid metabolism
p53 signaling pathway
Oxytocin signaling pathway
alpha-Linolenic acid metabolism
Serotonergic synapse
Pathways in cancer
Transcriptional misregulation in cancer
Circadian rhythm
0
1
2
- Log10 pValue
c
Log2FC
-1.12
1.12
OGT
PRMT5
AHR
RBM4
CREM
MTA1
HDAC3
PRKG2
PER3
ATF4
NCOA2
PPARGC1A
KMT2A
BHLHE40
NPAS2
PER2
NCOR1
CRY2
PPP1CA
NRIP1
PPARA
ARNTL
CLOCK
BHLHE41
HDAC1
HDAC2
CRY1
PPP1CC
SIRT1
NR1D1
CSNK1D
CSNK1E
PML
RORA
PER1
PPP1CB
RAI1
RORC

a

	Spearman rho	p-Value
UP in FASTING all genes /H3K9-bhb peaks (F vs AL)	0.13	4.4E-16
UP in FASTING only p<0.05/H3K9-bhb peaks (F vs AL)	0.19	6.7E-09

b

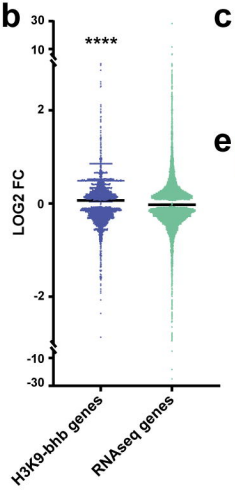

c

	Spearman rho	p-Value
UP in AD LIBITUM all genes /H3K9-bhb peaks (F vs AL)	0.0008	0.96
UP in AD LIBITUM only p<0.05/H3K9-bhb peaks (F vs AL)	-0.02	0.41

d

PROMOTERS	Spearman rho	p-Value
UP in FASTING all genes /H3K9-bhb on promoters (F vs AL)	0.13	4.4E-16
UP in FASTING only p<0.05/H3K9-bhb on promoters (F vs AL)	0.19	6.7E-09

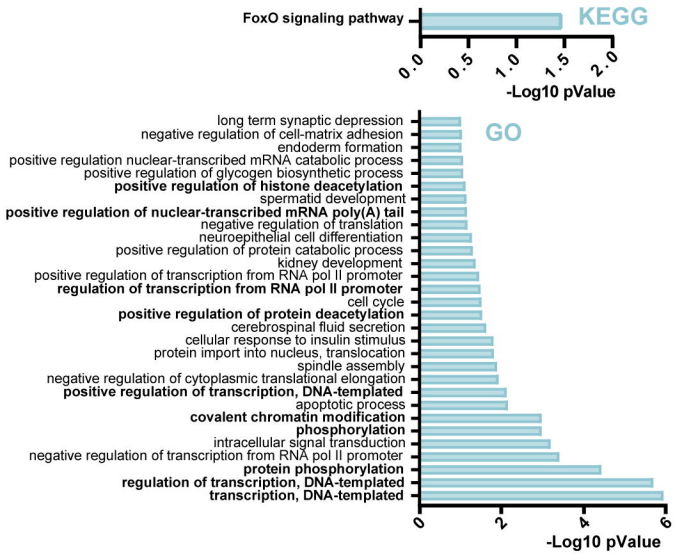

e

ENHANCERS	Spearman rho	p-Value
UP in FASTING all genes /H3K9-bhb on enhancers (F vs AL)	0.09	0.01

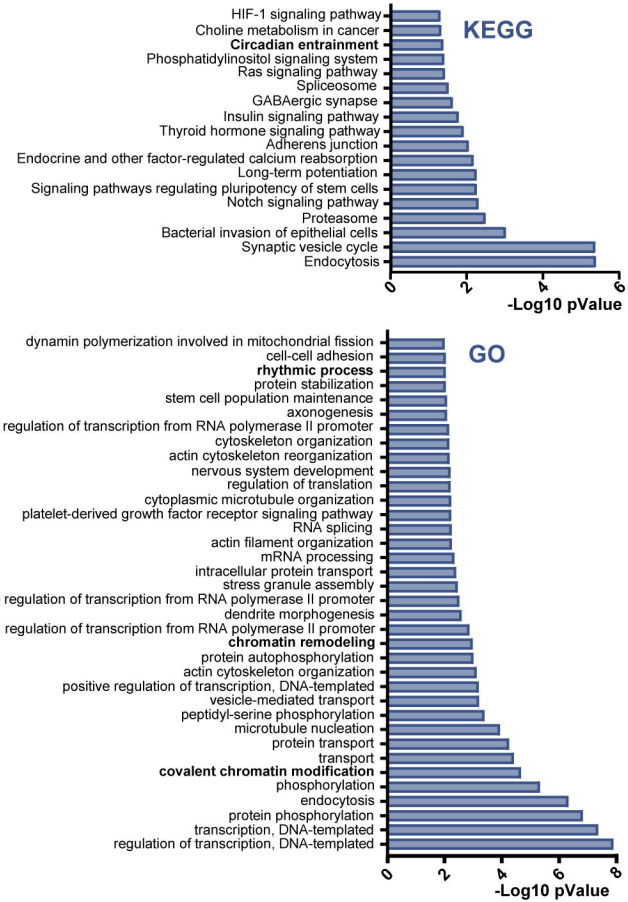

f

INTERGENIC REGIONS	Spearman rho	p-Value
UP in FASTING all genes /H3K9-bhb on intergenic regions (F vs AL)	0.16	0. 02

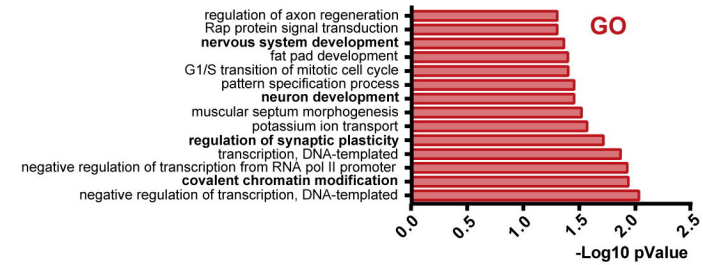

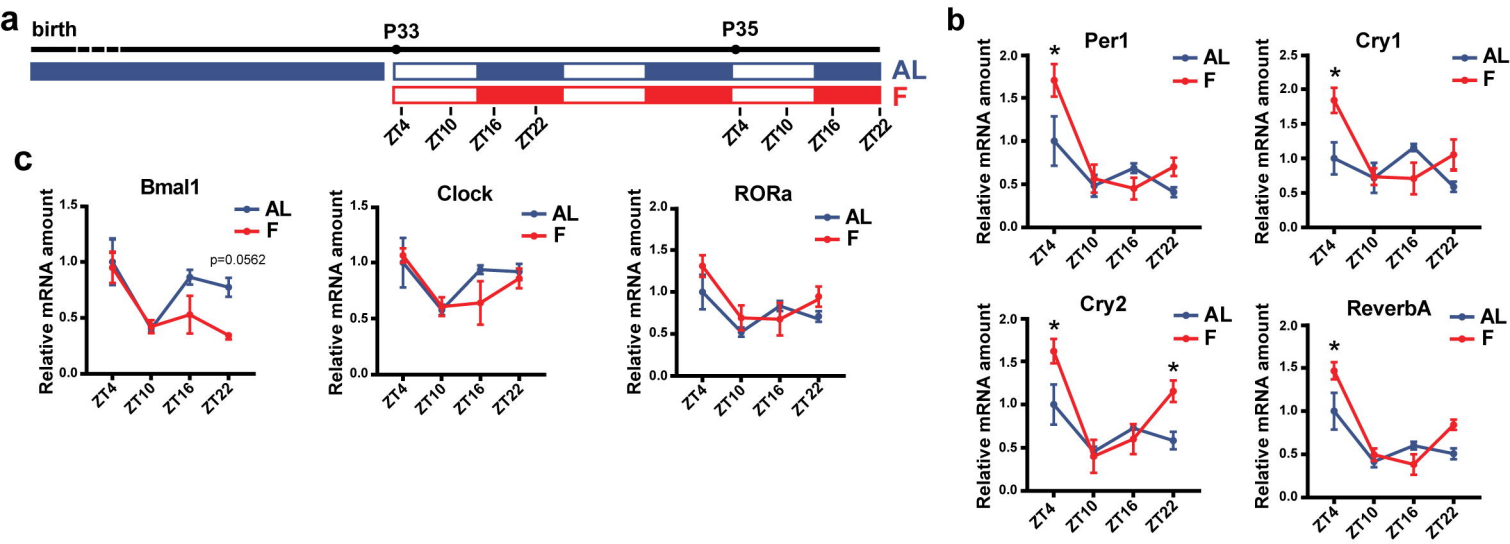
a
birth
P33
P35
AL
F
ZT4
ZT10
ZT16
ZT22
ZT4
ZT10
ZT16
ZT22
b
Per1
Cry1
Cry2
ReverbA
Relative mRNA amount
AL
F
*
c
Bmal1
Clock
RORa
p=0.0562
Relative mRNA amount
AL
F
ZT4
ZT10
ZT16
ZT22